Received: 29 January 2022 | Revised: 10 June 2022 | Accepted: 10 June 2022 | Published on: 27 June 2022

DOI: 10.1002/joc.7758

RESEARCH ARTICLE

International Journal of Climatology RMetS

Convective precipitation over a Mediterranean area: From identification to trend analysis starting from high-resolution rain gauges data

Dario Treppiedi | **Giuseppe Cipolla** | **Leonardo Valerio Noto**

Dipartimento di Ingegneria, Università degli Studi di Palermo, Palermo, Italy

Correspondence
Dario Treppiedi, Dipartimento di Ingegneria, Università degli Studi di Palermo, Palermo, Italy.
Email: dario.treppiedi@unipa.it

Abstract

Heavy rainfall events are likely to become more frequent and severe in the next future, under the effects of a changing climate. In this context, the scientific literature is characterized by a relevant number of studies trying to identify the convective component of precipitation, since this kind of phenomena, due to their short duration and high intensity, may lead to an increased risk of flash floods or debris flows and, consequently, human life losses and economic damages. In this study, a separation between the convective and stratiform precipitation, starting from the subhourly precipitation time series recorded over Sicily (Italy), is provided on a monthly scale. Results show that the percentage of convective precipitation increases as the associated intensity increases, following what is generally known about convective events. Moreover, during the summer months, higher percentages of convective rainfall are generally reached for lower values of intensity, since this season favours the occurrence of these phenomena due to high temperature and relative humidity. In addition to the regional analysis, even an at-site analysis has been carried out, through the definition of a critical intensity threshold to identify the predominant convective component for each rain gauge. This analysis has pointed out that such convective events have occurred mainly in the east part of the island mainly due to the complex orography of this area, which favours the occurrence not only of such phenomena but of flash floods and debris flows as well.

KEYWORDS

climate change, convective precipitation, high-resolution data, Mediterranean area, trend analysis

1 | INTRODUCTION

During the last decades, the scientific community has gathered a great number of evidence that humanity is experiencing a changing climate. The rise in global temperature has been extensively documented, as well as its direct influence on the hydrological cycle and the precipitation field (Kundzewicz, 2008; Trenberth, 2011; Donat *et al.*, 2016; Lionello and Scarascia, 2018).

Since during extreme rainfall events, all water vapour in the air (or a relevant and constant fraction of it) is converted into rain, then precipitation for extreme events is expected to scale with the Clausius–Clapeyron relation rate (i.e., 6–7%·°C^{-1}); however, it has already been demonstrated that this value is higher in some parts of the globe, and, particularly, in Europe (Lenderink and van Meijgaard, 2008; Ali *et al.*, 2021; Fowler *et al.*, 2021), thus leading to higher severity of heavy rainfall. Not only the magnitude but also the occurrence of intense precipitation is likely to increase in the future (Scoccimarro *et al.*, 2013; IPCC, 2019), incrementing the risk of severe flooding especially when hitting small catchments, characterized by low times of concentration (Borga *et al.*, 2007; Aronica *et al.*, 2012; Forestieri *et al.*, 2016) and highly urbanized (Aronica *et al.*, 2002; Pumo *et al.*, 2017; Arnone *et al.*, 2018). Concerning the Mediterranean area, many studies show that there has been an increase in short-duration and high-intensity rainfall events (Kyselý *et al.*, 2012; Arnone *et al.*, 2013; Bartolini *et al.*, 2014; Forestieri *et al.*, 2018; Treppiedi *et al.*, 2021). In this context, since event duration and intensity are strictly related to the mechanisms that generate the precipitation, a topic that has often been a source of interest is the one related to the classification of precipitation into stratiform and convective components (Tremblay, 2005; Ruiz-Leo *et al.*, 2013; Feloni *et al.*, 2019; Cipolla *et al.*, 2020) and, consequently, to the identification of convective events (Tremblay, 2005; Feloni *et al.*, 2019; Sottile *et al.*, 2021) and the detection of any trend in their characteristics (Rulfová and Kyselý, 2014; Llasat *et al.*, 2021).

At the spatial scale starting from the radar echoes, Houze (1997) defines the convective regime as the precipitation associated with young and active atmospheric convection. In this condition, the strong updraft that condenses a large amount of water in the air generates cumulus and cumulonimbus clouds and the related precipitation is generally characterized by short-duration and high-intensity (Llasat, 2001; Berg *et al.*, 2013; Westra *et al.*, 2014). On the other hand, stratiform precipitation occurs in a different atmospheric condition, namely when the convection is weak and the air motions are lower, thus producing precipitation events with opposite characteristics to the previous. Although the physical mechanisms that generate convective and stratiform precipitation have been widely discussed in the past, separating the two regimes is not trivial. Indeed, the convective and stratiform precipitation could occur separately or as a part of the same complex of clouds, not allowing a net distinction between the regimes (Houze, 1997; Tremblay, 2005; Rulfová and Kyselý, 2013; Kyselý *et al.*, 2016).

Nevertheless, over the years the issue of a correct distinction between precipitation in convective and stratiform components has been carried out from different points of view. The first attempts to deal with such a separation were mostly concerned with the spatial aspect of the problem, that is, to distinguish between convective and stratiform regions using weather radar imagery or remote sensing techniques (Steiner *et al.*, 1995; Reudenbach *et al.*, 2001; Rigo and Llasat, 2004; Sandford *et al.*, 2017).

Concerning the distinction of precipitation regimes on the base of ground observations, Tremblay (2005) analysed precipitation data of about 3,500 rain gauges collected by the World Meteorological Organization (WMO) at the global scale, setting up an algorithm for the classification of convective and stratiform precipitation components. The study revealed that the relationship between cumulative precipitation and its intensity can be described by a negative exponential law, independently from the period under study and the time step used to cumulate the raw rainfall data. Starting from this finding, Tremblay (2005) based the classification of the total precipitation into convective and stratiform components by assuming that the exponential curve corresponds with the stratiform component, while the difference between the total precipitation and exponential curves provides the convective component; moreover, the author define a rainfall intensity threshold to classify, at the gauge scale, as convective (stratiform) all the events with an intensity higher (lower) than that threshold. Ruiz-Leo *et al.* (2013) applied a similar algorithm to the 6-hr rainfall data recorded from 1998 to 2008 by 12 rain gauges located on the northeastern Mediterranean coast of Spain. The authors confirmed the above-mentioned assumption of Tremblay (2005), namely that an exponential distribution is observed when the total rainfall depth is represented versus the rainfall intensity. Considering both the annual and the seasonal convective precipitation, the application of a trend analysis reveals a significant increase in such a variable in the autumn. Feloni *et al.* (2019) applied the same approach presented in Tremblay (2005) to 6-hr rainfall time series of 32 rain gauges in the Attica region (Greece), obtained by aggregating the original 10-min rainfall time series in the period 2005–2015. The authors identified the critical intensity thresholds for each year under study, to detect the convective events and evaluate the annual fraction of convective rainfall. Moreover, results were validated using some indices representative mainly of the convective component, such as the lightning activity, which is very common in presence of cumulonimbus clouds that generate convective events. The validation procedure highlights how the separation algorithm is characterized by high performance in

classifying the correct type of precipitation, thus providing a useful tool to identify convective rainfall in gauged sites.

Starting from the rainfall annual maxima at fixed durations (1, 3, 6, 12, and 24 hr) for Sicily (Italy), Cipolla *et al.* (2020) developed a criterion to classify annual maxima between convective and stratiform, also taking into account a third class containing mixed/unresolved events, by means of two reanalysis indexes, namely the Convective Available Potential Energy (CAPE) and the Vertical Integral of Divergence of Moisture Flux (VIDMF) retrieved by the ERA-Interim archive. The authors found that, in general, at 1-hr duration, the percentage of convective events predominates in the other classes of events mainly in the summer season, while the percentage of stratiform tends to increase at 24-hr duration during the winter period. The significant percentage of mixed/unresolved annual maxima, which is recognized at all durations, highlights the presence of many rainfall events which could be classified as both convective and stratiform events or do not show a sufficiently clear distinction between the two classes.

In this work, starting from the SIAS (Servizio Informativo Agrometeorologico Siciliano) database for Sicily in the period 2002–2020, 20-min precipitation time series have been created from high-resolution rainfall time series and then used to (a) separate the convective and the stratiform precipitation at a 5-day scale according to the framework proposed by Tremblay (2005), (b) determine a critical threshold able to identify the predominant convective events at at-site scale in the whole period under study and, (c) investigate the spatial pattern relative to the occurrence and the percentage of convective events and their possible trend.

The paper is structured as follows: a brief description of the area under study, along with the involved rainfall database and the methodology, is presented in section 2. Section 3 provides a description and some comments about the results. Finally, in section 4 some conclusions concerning the study are summarized.

2 | MATERIAL AND METHODOLOGY

2.1 | Study area and dataset

Sicily, with an area of 25,700 km^2, is the largest island in the Mediterranean Sea. The island is characterized by great variability in elevation. Precipitation varies a lot across the island, both spatially and temporally; more specifically, the Mean Annual Precipitation (MAP) is lower in the southeast (360 mm on average) and higher in the northeast (1,900 mm on average) of the region (Di Piazza *et al.*, 2011). From a temporal point of view, winter is usually affected by the greatest part of the annual precipitation, while summer generally manifests relevant dry periods, even if severe storms, such as the one that recently occurred in Palermo on 15th July 2020 (Francipane *et al.*, 2021), may sometimes occur in this season.

The precipitation dataset used in this study has been provided by the regional agency SIAS (Servizio Informativo Agrometeorologico Siciliano). The database comes from about 100 rain gauges, uniformly distributed across the island and with an average density equal to about 250 km^2/gauge (Figure 1). The location of all the gauges under study, overlaid with the Digital Elevation Model (DEM) of the region, is shown in Figure 1. The rain gauge network, as stated by the SIAS agency, complies with the WMO requirements in terms of site selection, data detection, management, and validation criteria. All these aspects ensure a high level of homogeneity in the rainfall time series. The gauges have been continuously collecting rainfall data at the 10-min resolution for about 20 years. In particular, the data considered in this study cover the period between January 2002 and December 2020 (i.e., 19 years) for almost 80 stations, while for the remaining gauges, data are mainly available for a shorter period but until December 2020.

The original 10-min rainfall time series have been aggregated to the 20-min resolution by dividing the whole period into not overlapping 20-min intervals and cumulating the rainfall depth within them; in this way, the amount of rainfall that occurred in 20 min, namely an average intensity of precipitation (e.g., mm·20 min^{-1}) has been derived. Compared to the original 10-min resolution, the choice of 20-min time resolution increases the probability that single-cell thunderstorms peaks are included in a single interval since individual cell life cycle is generally between 30 and 60 min (NOAA, 2012). At the same time, the high resolution of the available dataset is maintained, being a novelty compared to the previous studies (Tremblay, 2005; Ruiz-Leo *et al.*, 2013; Feloni *et al.*, 2019), in which time series have been used with a frequency of 6 hr. Indeed, while considering 6-hr intervals could be a good compromise when convective and stratiform contributions are analysed at a global scale, such as in Tremblay (2005), it is necessary to use finer resolution when the studied area is limited, such as in the case of Sicily. There is also evidence that convective precipitation can develop in time intervals significantly shorter than 6 hr (Llasat, 2001; Hardwick Jones *et al.*, 2010; Berg *et al.*, 2013).

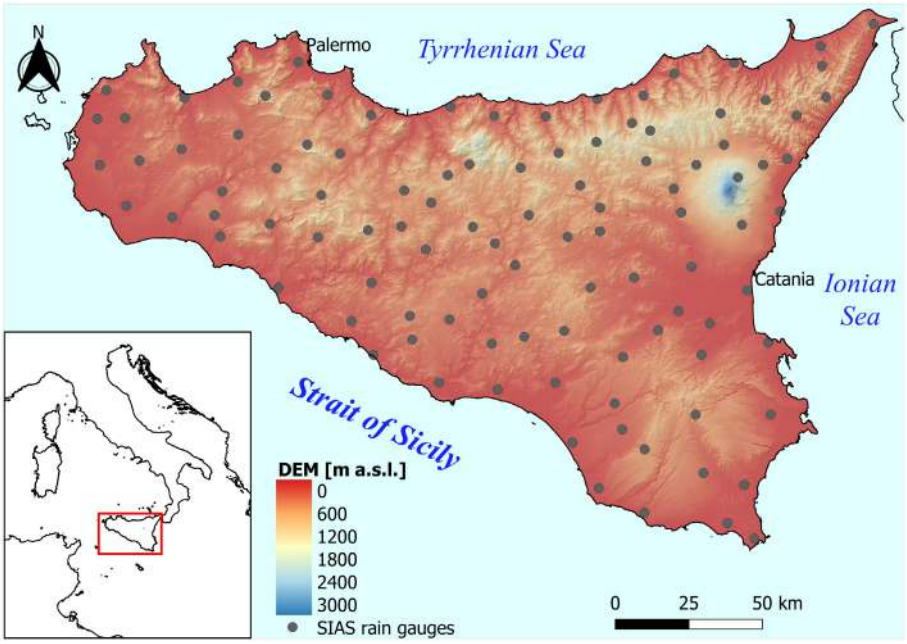

FIGURE 1 Spatial distribution of SIAS rain gauges, overlaid to the digital elevation model (DEM), for Sicily [Colour figure can be viewed at wileyonlinelibrary.com]

2.2 | The partitioning procedure

This study aims to separate the stratiform and the convective component of precipitation on a monthly scale, by using the framework proposed by Tremblay (2005). The first step consists of defining an empirical total precipitation distribution ($P_T(I)$), considering a specific average time interval $\Delta\tau$. Then, a negative exponential curve is fitted to model the stratiform precipitation component ($P_S(I)$). The convective component is therefore defined by the difference between the total precipitation and the stratiform components. A detailed explanation of this procedure can be found in the following subsections.

2.2.1 | The total precipitation distribution

As mentioned in the previous paragraph, obtaining the empirical total precipitation distribution is essential to distinguish the stratiform component and, consequently, also the convective one. To derive the monthly $P_T(I)$, a pre-processing procedure is required.

The first step aims to remove the dependency of the data on the location of the rain gauges. Indeed, the separation between the two regimes takes place on a spatial scale defined by the available ground observations. For example, Tremblay (2005) applied the algorithm on a global scale, while the goal of this study is to work at a higher spatial resolution, defined over Sicily. Nevertheless, our study area is larger than the one used by Ruiz-Leo *et al.* (2013) (i.e., a part of the Spanish Mediterranean coast and the Balearic Island) and Feloni *et al.* (2019) (i.e., the Attica peninsula). To move from an at-site to a regional scale, the data recorded by all the gauges in the same 20-min interval (i.e., corresponding with Δt) needs to be gathered on the base of their rainfall intensity. With this purpose, an intensity bin size, namely ΔI, is used to define a certain number of intensity classes, obtained by dividing the intensity range of variability by ΔI. Hence, the empirical total precipitation distribution $P_T(I)$ for the considered time interval Δt is obtained by grouping and cumulating the rainfall data according to the intensity class to which they belong. More specifically, the latter $P_T(I)$ describes how the total rainfall depth is distributed with the intensity, in a specific Δt. It is important to specify that such a distribution is derived for the region under study as a whole as previously stated (e.g., no spatial information is included in the empirical total precipitation distribution $P_T(I)$).

Before applying the partitioning algorithm, it is necessary to choose an average time interval, $\Delta\tau$, to which the analysis is referred. The first way may consist in considering a $\Delta\tau$ equal to the time series resolution Δt, such as in Tremblay (2005), thus providing four empirical distributions per day for further partitioning ($\Delta t = \Delta\tau = 6$ hr). On the other hand, it is possible to choose $\Delta\tau > \Delta t$, such as the year (Ruiz-Leo *et al.*, 2013; Feloni *et al.*, 2019), or a 5-day scale here proposed. More specifically, 30-day months are divided into six identical intervals, while the last one contains (a) 1 day more in the case of 31-day months or (b) 2 days less in the case of February (or 1 day less for the leap years). This kind of subdivision has been preferred to a constant 5-day window so that each interval falls within a specific month, and therefore

it allows for analysing the monthly behaviour of the considered variables. To obtain the 5-day empirical $P_T(I)$, it is necessary to select all the 20-min distributions within the considered $\Delta\tau$ (i.e., 5 days in our case) and aggregate them at the same intensity classes. Through this aggregation procedure, the number of distributions per year is reduced from 26,280 (e.g., 72 distributions per day for a total of 365 days) to 72 (e.g., six per month), as it will be shown in section 3.1.

2.2.2 | The partitioning algorithm

According to Tremblay (2005), an exponential structure can be always detected by looking at total precipitation distributions, regardless of the $\Delta\tau$. Indeed, the total precipitation depth tends to decrease exponentially as the rainfall intensity class increases. From a statistical point of view, this is mainly connected to the relationship between the probability of occurrence of the rainfall events and their related severity. Indeed, the total volume of rain associated with events that occur frequently with lower intensities is probably higher compared to the one connected to a single very intense event. As explained by Tremblay (2005), this is a consequence of the fact that the rainfall intensity strictly depends on the residence time of particles in the clouds and, in turn, the probability of observing a certain residence time can be modelled with an inverse exponential distribution. For further details the Reader is referred to Tremblay (2005).

Moreover, Tremblay (2005) has shown that this exponential structure mainly prevails in correspondence of classes with lower intensity, while the total precipitation distribution generally exhibits an irregular behaviour for the higher intensities, as if some local peaks are superimposed to an exponential curve. Since it is realistic to assume that in these anomalies the convective component is significant, especially when the intensity of rainfall is relevant, it is possible to associate the exponential structure to the stratiform component and the anomalies with the convective one.

Starting from the previous considerations, for a certain $\Delta\tau$, the convective component of the precipitation can be obtained by subtracting a pure exponential curve from the total precipitation one,

$$P_C(I) = P_T(I) - P_S(I) = P_T(I) - a \cdot e^{-b \cdot I}, \qquad (1)$$

where $P_T(I)$ is the total precipitation distribution, $P_C(I)$ and $P_S(I)$ are the convective and the stratiform component, respectively, while a and b are the parameters needed to model the latter. Since the above-mentioned distributions have been defined as time scale dependent, it is worth highlighting that each term in Equation (1) is a function of the $\Delta\tau$ fixed. For the 5-day scale approach, 72 couple of parameters (namely a and b) must be derived per year.

Since mathematical modelling cannot be separated from the physical phenomenon, these parameters need to be estimated after defining a series of constraints. Indeed, a stratiform component greater than the total precipitation would result in a negative convective component, which has no physical meaning. For this reason, the curve should pass through the relative minima of $P_T(I)$ or, when it is not possible, it must be fixed equal to $P_T(I)$, meaning that there is no convective contribution in the considered intensity class.

2.2.3 | Model dependencies

Before delving into the results, it is useful to focus the attention on some dependencies of the partitioning algorithm. The ability of the model to differentiate between the stratiform and the convective component of the precipitation depends not only on the ΔI, as highlighted by Ruiz-Leo *et al.* (2013) and Feloni *et al.* (2019), as well as the sample size and the $\Delta\tau$ as originally pointed out by Tremblay (2005).

Since ΔI represents the resolution required to describe the total precipitation distribution, a greater intensity bin size may result in an excessively smooth curve, thus reducing the accuracy of the algorithm in identifying convective rainfall. On the contrary, even if one may think that the smaller this value, the greater the capability of the algorithm to separate the two regimes, and since the exponential curve is forced to pass through the minima of $P_T(I)$, an excessive number of local peaks or anomalies following Tremblay (2005) could lead to an overestimation of the convective component.

To overcome this issue, Ruiz-Leo *et al.* (2013) proposed a criterion useful to choose ΔI according to a parameter, derived from the standard deviation of precipitation intensity and the number of no-null precipitation data for all the gauges considered. Nevertheless, this empirical method for choosing ΔI has been probably calibrated for the annual $\Delta\tau$, leading to unrealistic results in the case of lower $\Delta\tau$. This is especially true for the driest months, in which the standard deviation is high and the resulting ΔI is excessively wide to separate the regimes. Since in this work a high-resolution dataset is used, four different values of ΔI have been tested. In particular, it has been fixed equal to 0.6, 1, 1.4, and 1.8 mm·20 min^{-1} and then applied to discretize the total precipitation distribution $P_T(I)$ for each 5-day interval.

Another parameter that influences the algorithm is the $\Delta\tau$. In particular, Tremblay (2005) proved that, for fixed sample numerosity, the greater the $\Delta\tau$ (e.g., 6 hr, 1 day, 1 month, 1 year), the smoother the total precipitation distribution $P_T(I)$, tending to a perfect exponential distribution. From a statistical point of view, this evidence is explained by the fact that a higher $\Delta\tau$ value implies that a greater number of events are aggregated in each intensity class and, at the same time, that it is likely that low-intensity events occur more frequently than high-intensity ones.

The opposite effect could be reached by considering, for a fixed $\Delta\tau$, a lower sample size. This could occur if data are aggregated using a higher time window (e.g., using the 1- or 6-hr time resolution to obtain the hourly or the hexa-hourly rainfall time series, instead of the 20-min resolution) or even if a decreasing number of stations is available. As an example, Ruiz-Leo *et al.* (2013) and Feloni *et al.* (2019) were forced to choose the annual $\Delta\tau$ because of the small number of rain gauges involved (i.e., 12 and 11 on average, respectively) even if the authors do not explicitly mention this aspect in their works, while, on the opposite Tremblay (2005) was able to apply the algorithm for a 6-hr $\Delta\tau$ because of availability of a global rain gauges network.

For this reason, the 5-day $\Delta\tau$ can be considered as a good trade-off between sample size and average time interval in the case of this work, as indicated from the analysis over different time averaged periods conducted by Tremblay (2005). Indeed, the use of a higher $\Delta\tau$ (e.g., the month) could result in excessive smooth empirical total precipitation distribution $P_T(I)$, while choosing a lower $\Delta\tau$ (e.g., the day) could lead to an opposite behaviour and to a higher probability of not having rainfall depth within the fixed $\Delta\tau$, particularly during the driest months.

2.3 | Detection of convective events

As mentioned in the previous subsection, the spatial information of the precipitation is lost during the derivation of the empirical total precipitation distribution, $P_T(I)$, and the consequent partitioning technique. Indeed, since the separation between the convective and the stratiform regimes is carried out at the regional scale, it does not allow to identify for each rain gauge those events characterized by the predominance of the convective component.

To overcome this limit and pass from a regional to an at-site classification of the two components, Tremblay (2005) introduced a critical intensity threshold (hereinafter I_{cr}), representing the value of intensity from which the convective component begins prevailing on the stratiform one. In other words, starting from the results of the separation for the fixed $\Delta\tau$, the I_{cr} threshold splits the intensity domain into two parts: a first part where the stratiform prevails on the convective component for $I < I_{cr}$, and a second one where the convective is predominant for $I > I_{cr}$. Consequently, I_{cr} is defined as the first intensity value that ensures,

$$P_C(I_{cr}) > P_S(I_{cr}). \quad (2)$$

As pointed out by Ruiz-Leo *et al.* (2013), this criterion could lead to an important underestimation of the threshold, mainly because $P_C(I)$ could be locally greater than $P_S(I)$ for lower values of intensity, due to the exponential fitting. Therefore, this criterion has been subsequently modified by Ruiz-Leo *et al.* (2013) and Feloni *et al.* (2019). In particular, Ruiz-Leo *et al.* (2013) suggested that this threshold should be fixed when the convective component represents 60% of the total cumulative precipitation since Houze (1993) found that this percentage can be considered a characteristic of the convective rainfall in a Mesoscale Convective System (MCS). Nevertheless, it has been noticed that in Europe these organized complexes of cumulonimbus are characterized by different features (e.g., size and duration) compared to other parts of the world (Rigo and Llasat, 2007; Kolios and Feidas, 2010; Michaelides *et al.*, 2018) and are mainly continental (Morel and Senesi, 2002; Kolios and Feidas, 2010), suggesting that also other types of a thunderstorm (e.g., single- and multi-cell storms) need to be considered in deriving I_{cr} for Sicily. Feloni *et al.* (2019), instead, shifted the previous threshold from 60 to 50% of the total cumulative precipitation.

Nevertheless, considering cumulative convective precipitation among the intensity classes may misrepresent the results of the separation algorithm, since the convective and the stratiform amount of rainfall strictly depends on the intensity class to which they belong, as shown in Equation (1). Moreover, the convective rainfall corresponding to higher intensity is certainly associated with a different atmospheric mechanism than the one related to lower intensity values. For such reasons, a different method for obtaining I_{cr} is proposed in this paper. In particular, it has been noticed that the median value of the percentage of convective rainfall for a certain month and intensity increases as the intensity values increase, as a result of the partitioning procedure. Therefore, it is possible to set the monthly I_{cr} as the first intensity from which the median percentage of convective exceeds a certain value, which would mark it out as predominant on the stratiform regime (e.g., 50 or 75% whose effects are assessed in section 3.3).

2.4 | Mann–Kendall trend test

The nonparametric Mann–Kendall trend test (Mann, 1945; Kendall, 1948) is used to verify the presence of any significant trend in the analysed variables. In this test, the null hypothesis indicates that the population, from which the sample is extracted, is characterized by no trend. Consequently, the existence of a trend is represented by the alternative hypothesis. To accept or decline the null hypothesis at a fixed significance level (i.e., α_{sig}) a comparison between α_{sig} and a local significance level (i.e., p_{value}) is required. This last term is obtained as follows:

$$p_{value} = 2[1 - \Phi(|Z_S|)], \tag{3}$$

where $\Phi(\cdot)$ is the CDF (cumulative distribution function) of a standard normal variate. The standardized test statistic, Z_S, follows a standard normal distribution and can be computed as reported below:

$$Z_S = \begin{cases} \dfrac{S-1}{\sigma} & \text{if } S>0 \\ 0 & \text{if } S=0 \\ \dfrac{S+1}{\sigma} & \text{if } S<0 \end{cases}. \tag{4}$$

In Equation (4), σ is the variance of the standardized normal distribution function followed by the Kendall's S statistic, under the null hypothesis. The S statistic is computed as the sign function of the difference between two consecutive observations, namely x_i and x_j,

$$S = \sum_{i=1}^{n-1} \sum_{j=i+1}^{n} \operatorname{sign}(x_j - x_i). \tag{5}$$

The evaluation of trends can be also conducted at the regional scale through the regional Kendall test (Douglas *et al.*, 2000; Cannarozzo *et al.*, 2006; Helsel and Frans, 2006). The Kendall's S statistic is evaluated through Equation (5) at each location and then the average, S_m, is computed. The p-value is finally derived from Equation (3) after that the regional standardized test statistic, Z_R, is obtained as follow:

$$Z_R = \begin{cases} \dfrac{S_m-1}{\sigma_{Sr}} & \text{if } S>0 \\ 0 & \text{if } S=0, \\ \dfrac{S_m+1}{\sigma_{Sr}} & \text{if } S<0 \end{cases} \tag{6}$$

where σ_{Sr} takes into account the sample numerosity at each gauge through n_l,

$$\sigma_{Sr} = \sqrt{\sum_{l=1}^{m} \frac{n_l(n_l-1)(2n_l+5)}{18}}. \tag{7}$$

3 | RESULTS AND DISCUSSION

In this section, the methodology presented in section 2 is applied and the related results are presented and discussed. After a preliminary data preprocessing (section 3.1), the partitioning algorithm at the regional scale is applied to obtain the median percentage of convective events for each month (section 3.2). Finally, once the monthly critical rate intensity thresholds I_{cr} are obtained, the convective events at a site scale are identified, allowing to search for spatial patterns and perform trend analysis of their characteristics (section 3.3).

3.1 | Data preprocessing

The preprocessing of data, as described in section 2.1, is fundamental to derive the empirical total precipitation distribution $P_T(I)$. In particular, the 20-min rainfall intensity time series of all the gauges have been combined and gathered in rainfall intensity classes, whose width ΔI has been fixed in section 2.2.3. As an example, Figure 2 shows a comparison between the cumulative precipitation heatmap (i.e., a 2D matrix where the magnitude of the variable of interest in each cell is represented through a colour scale) for (a) February and (b) September of the year 2006, considering (1) $\Delta I = 0.6\,\text{mm}\cdot 20\,\text{min}^{-1}$ and (3) $\Delta I = 1.8\,\text{mm}\cdot 20\,\text{min}^{-1}$, which are the upper and lower bounds of the interval analysed. Considering a generic 20-min time interval (on the x-axis), for each intensity class (on the y-axis), the colours from red to blue represent the total precipitation recorded by all the rain gauges within that class. The black colour, instead, is used to mark those time intervals in which no events in the intensity class have been recorded. The subpanels inside each heatmap provide a zoom of a specific day (i.e., 23rd February 2006 and 15th September 2006) for (2) $\Delta I = 0.6\,\text{mm}\cdot 20\,\text{min}^{-1}$ and (4) $\Delta I = 1.8\,\text{mm}\cdot 20\,\text{min}^{-1}$. Panels (c) and (d), instead, show the 20-min total precipitation distribution for two dates (i.e., black colour for 1500 LST (UTC+) of the 15th of September 2006 and red colour for 1700 LST of the 23rd of February 2006) related to $\Delta I = 0.6\,\text{mm}\cdot 20\,\text{min}^{-1}$ and $\Delta I = 1.8\,\text{mm}\cdot 20\,\text{min}^{-1}$,

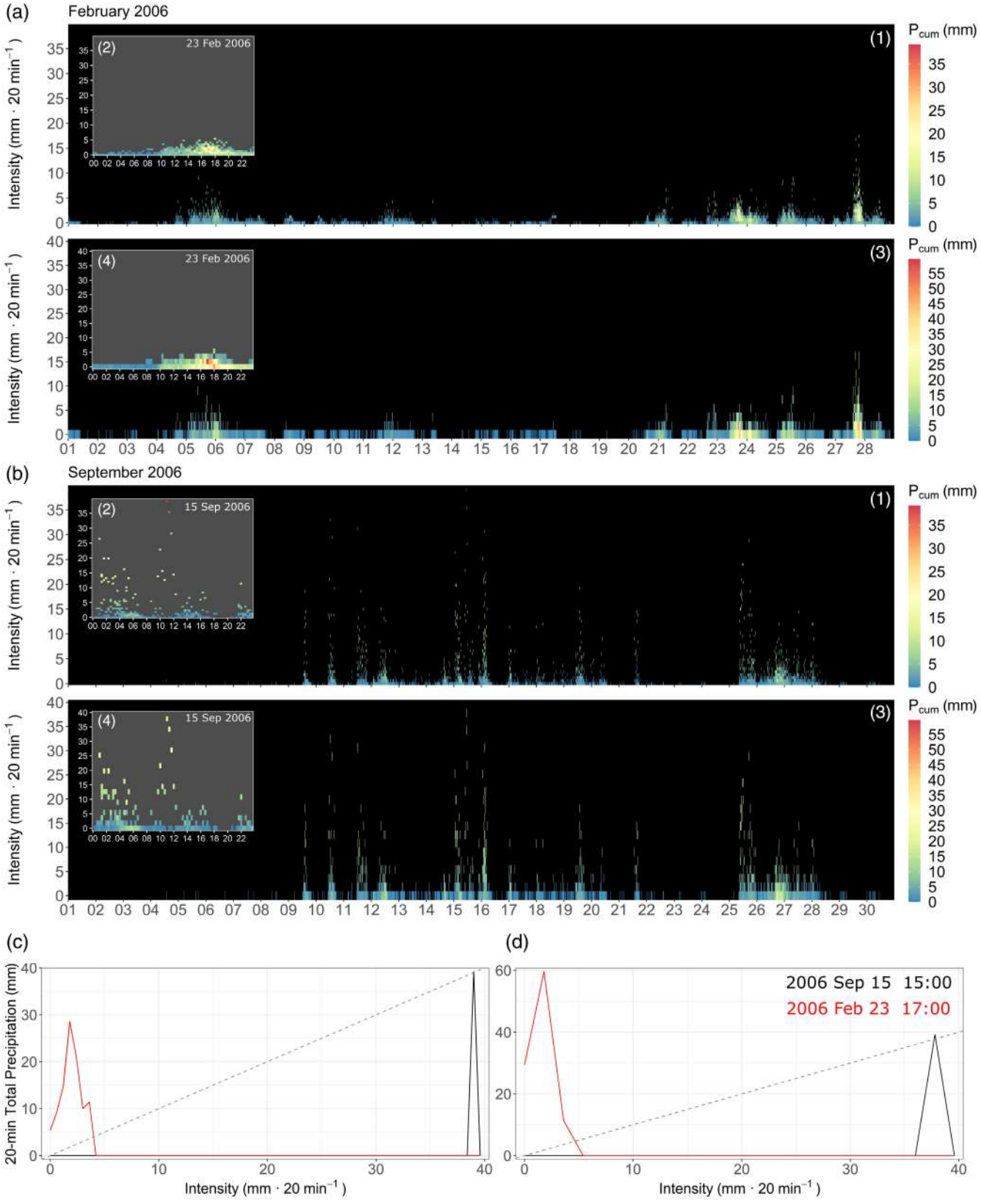

FIGURE 2 Precipitation intensity heatmap for (a) February and (b) September of the year 2006 at (1) $\Delta I = 0.6$ mm·20 min^{-1} and (3) $\Delta I = 1.8$ mm·20 min^{-1}. The colourbar in the right indicates the total precipitation values. The black colour indicates that no rainfall events are recorded within the considered intensity interval. The subpanels inside each heatmap provide a zoom for 23rd February 2006 and 15th September 2006 for (2) $\Delta I = 0.6$ mm·20 min^{-1} and (4) $\Delta I = 1.8$ mm·20 min^{-1}. The 20-min precipitation distribution related to the 1500 LST of the 15th September 2006 (black curve) and to the 1700 LST of the 23rd February 2006 (red curve) are depicted for (c) $\Delta I = 0.6$ mm·20 min^{-1} and (d) $\Delta I = 1.8$ mm·20 min^{-1} [Colour figure can be viewed at wileyonlinelibrary.com]

respectively, while the grey dashed line is the perfect agreement line. In other words, the black and red curves are representative of two columns of the above heatmaps, and the single rainfall events lying on the perfect agreement line are characterized by the same value of intensity and cumulative precipitation.

For both the months and especially at the lower ΔI (panels a_1 and b_1), three different regions can be identified as a function of intensity; indeed, focusing on the lower intensity, it is possible to notice that the blue prevails on the other colours and even on the black, meaning that the total precipitation is generally low but, at the same time, it is more frequent across the month. As a result of the heatmap definition procedure, these total precipitation values consider a high number of very low intensity events that are recorded in the entire region during the month. As the intensity increases, the total precipitation assumes greater values but with a lower occurrence frequency, thus defining an intermediate region where the yellow colour is noticeable, especially in some spikes, representing those temporal intervals in which the whole region was interested in more severe rainfall events. Finally, in the zone characterized by the higher values of intensity, the rainfall events are particularly rare, and black becomes the main colour (i.e., no-occurrence). Moreover, these events are generally due to single high-intensity precipitation, as it is visible also in panel (c) and (d), and they are probably dominated by a convective component. It is also important to highlight that these kind of spikes in the heatmaps are more frequent in September rather than in February, as featured by the daily enlargements. From a physical point of view, this is probably caused by the different climatic conditions in these 2 months, which implies that a seasonality in the occurrence of convective/stratiform events needs to be analysed.

The effect of the selection of a wider ΔI is evident moving from panel (1) to panel (3) for both months. Indeed, with a higher ΔI, the resolution of the heatmap worsen, even if the global appearance is maintained. Moreover, as a result of a wider intensity class, the maximum total precipitation is likely not to be found in the higher intensity classes, as it is possible to notice in the daily zooms and, contemporary, in panels (c) and (d). Indeed, while for $\Delta I = 0.6$ mm·20 min^{-1} the maximum value (i.e., about 40 mm) occurs in mid-September with an intensity equal to 40 mm·20 min^{-1}, the highest total precipitation for $\Delta I = 1.8$ mm·20 min^{-1} (i.e., about 60 mm) occurs the 23rd of February with an intensity value of 3.6 mm·20 min^{-1}. As depicted in panels (c) and (d), this aspect is strictly connected to the ΔI width: considering the smaller ΔI (panel c), the single high-intensity event (about 40 mm·20 min^{-1}) recorded on the 15th of September 2006 (the black curve) corresponds to the maximum value of the total precipitation; by enlarging the ΔI to 1.8 mm·20 min^{-1} (panel d), the events recorded on the 23rd of February 2006 (the red curve) and characterized of intensity around 3.6 mm·20 min^{-1} fall into the same class, so that a total precipitation value greater than 40 mm is achieved.

Furthermore, focusing on panels (c) and (d) it is possible to notice that the 20-min total precipitation distributions are excessively discrete and do not always follow a negative exponential curve for both $\Delta I = 0.6$ mm·20 min^{-1} and $\Delta I = 1.8$ mm·20 min^{-1}, not allowing the partitioning procedure as stated in Tremblay (2005).

For this reason, the heatmaps shown in Figure 2 can be considered a practical instrument to understand whether it is possible to use the partitioning algorithm directly, or it is first necessary to set a higher $\Delta\tau$. In the case of this work, after fixing $\Delta\tau$ equal to the 5-day scale, the total precipitation within each 5-day window has been aggregated for each intensity class (i.e., across the rows of the heatmap).

The results of such a procedure are shown in Figure 3, where the 5-day total precipitation heatmaps related to the year 2006 are presented, in a similar manner to Figure 2, for (a) $\Delta I = 0.6$ mm·20 min^{-1} and (c) $\Delta I = 1.8$ mm·20 min^{-1}. The same figure shows the 5-day $P_T(I)$ related to the periods (1) 21–25 January, (2) 11–15 June, (3) 26–31 August, and (4) 21–25 November and for three different ΔI: (a) 0.6 mm·20 min^{-1}, (b) 1 mm·20 min^{-1}, and (c) 1.8 mm·20 min^{-1}.

As it is possible to observe from the heatmaps (a) and (c), the aggregation procedure generates a monthly total precipitation distribution generally decreasing with the intensity, in clear contrast with the 20-min $P_T(I)$ shown in panels (c) and (d) of Figure 2. It is worth to observe that this behaviour is more evident for the 5-day intervals related to the winter months (i.e., from December to March), where a high $P_T(I)$ at the lower intensities is due to a high number of low-intensity events, which typically occur in such a period. On the contrary, the ones within the months from May to August are generally drier and, for this reason, the 5-day $P_T(I)$ in the lower intensity classes assumes smaller values if compared to those in the winter months. However, a pattern decreasing with the intensity is maintained.

These aspects are enhanced by looking at the distributions for the four 5-day intervals shown in panels (a_1–a_4), (b_1–b_4), and (c_1–c_4). As an example, passing from January to June and August, it is possible to notice an important reduction in the integral of the curves which represents the total rainfall recorded in the considered time interval, despite some spikes in correspondence of higher

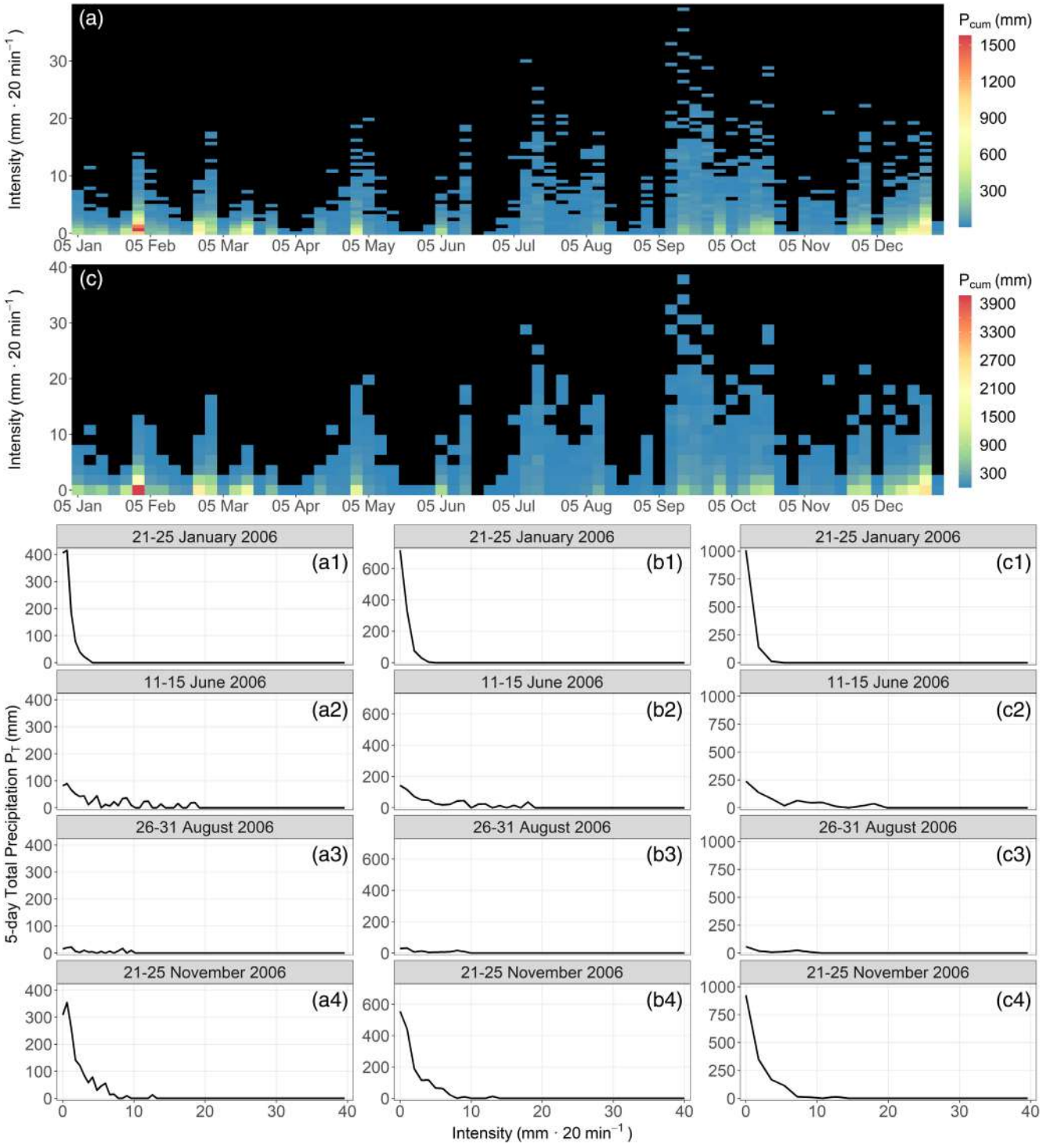

FIGURE 3 Precipitation intensity heatmap for the year 2006 at the 5-day scale (a) $\Delta I = 0.6$ mm·20 min^{-1} and (c) $\Delta I = 1.8$ mm·20 min^{-1}. The colourbar on the right indicates the total precipitation values within the intervals. The black colour indicates that no rainfall events are recorded within the considered intensity interval in the considered 5-day interval. The remaining panels show the $P_T(I)$ for (1) 21–25 January, (2) 11–15 June, (3) 26–31 August, and (4) 21–25 November combined with (a) $\Delta I = 0.6$ mm·20 min^{-1}, (b) $\Delta I = 1$ mm·20 min^{-1}, and (c) $\Delta I = 1.8$ mm·20 min^{-1} [Colour figure can be viewed at wileyonlinelibrary.com]

intensities are present. In other words, even if the amount of low-intensity precipitation clearly decreases in June, and August, this does not happen with the high-intensity events. This can be considered a consequence of the fact that these months are generally drier but, at the same time, they are proportionally more characterized by

high-intensity events. Finally, concerning the 5-day interval related to November, the general behaviour of the total precipitation distribution is more similar to the one in January, even if some high-intensity spikes can be identified between 5 and 15 mm·20 min^{-1}.

Passing from the first to the third column of Figure 3, the main consequence of a wider ΔI is that the total precipitation distribution becomes smoother and smoother. Furthermore, by observing the $P_T(I)$ curves related to 21–25 November (i.e., panels a_4–c_4), it is noteworthy that the maximum value of $P_T(I)$ is not always reached in the first intensity class. This aspect, in general, tends to become less important or disappear as ΔI increases.

3.2 | Partitioning procedure

The application of the partitioning algorithm to the 5-day precipitation distribution allows classifying the percentage of convective and stratiform components considering all the intervals in the period 2002–2020. Figure 4 shows the results of the algorithm described in section 2.2.2 when applied to the same cases of Figure 3, namely (1) 21–25 January, (2) 11–15 June, (3) 26–31 August, and (4) 21–25 November of the year 2006, for (a) ΔI = 0.6 mm·20 min^{-1}, (b) ΔI = 1 mm·20 min^{-1}, and (c) ΔI = 1.8 mm·20 min^{-1}. The black and the red solid lines represent the total precipitation distribution and its stratiform component represented by the negative exponential curve, respectively, while the convective amount of rainfall for each class of intensity is depicted with the grey bars.

At a first sight, the results seem to confirm that the algorithm is not significantly affected by the ΔI considered. Indeed, by observing the convective bars for the whole panels, it is possible to notice that these are mainly located in the right part of the total precipitation distribution, namely that there is a predominant convective rainfall at high rainfall intensity classes. This aspect confirms what Tremblay (2005) affirmed about the characteristics of convective precipitation, such that for a certain duration (i.e., 20 min in the case of this study) it is likely that the convective precipitation is generally characterized by higher intensity values. Moreover, this aspect is enhanced

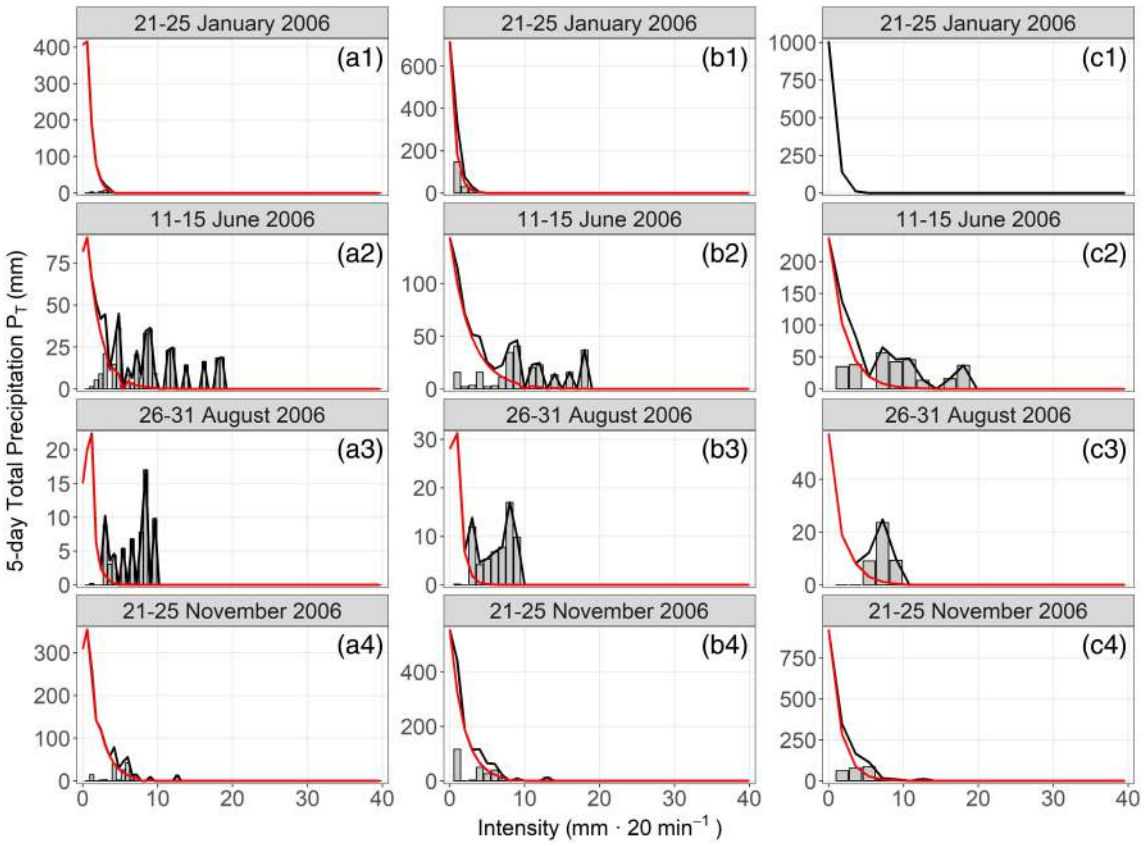

FIGURE 4 Results from the application of the partitioning procedure for the same combinations between 5-day interval and ΔI depicted in Figure 3. The black lines represent the 5-day total precipitation distribution, while the red lines stand for the stratiform component (i.e., the negative exponential curve). The grey bars, instead, quantify the convective amount of rainfall for each class of intensity [Colour figure can be viewed at wileyonlinelibrary.com]

for the 5-day windows in the driest months (i.e., June and August), confirming what other authors have found about a greater occurrence of convective events during the summer months. As an example, Sottile *et al.* (2021) found a seasonality in the percentage of convective events in Sicily, with the highest ones from May to October, despite the authors used a different framework and pre-processing of data. Concerning other regions in the Mediterranean Muñoz-Díaz and Rodrigo (2006) indicate the important role of local and convective processes in the summer and autumn seasons for Spain, as well as Nastos *et al.* (2014) suggest that these seasons are more interested in convective events due to the high lightning activity.

Nevertheless, it is also possible to affirm that a lower ΔI would be excessively close to the resolution of the gauges used (i.e., 0.2 mm·20 min^{-1} for the SIAS network) and, during the aggregation procedure, an excessively jagged pattern of the total precipitation distribution would be generated, resulting in a difficult fitting of a

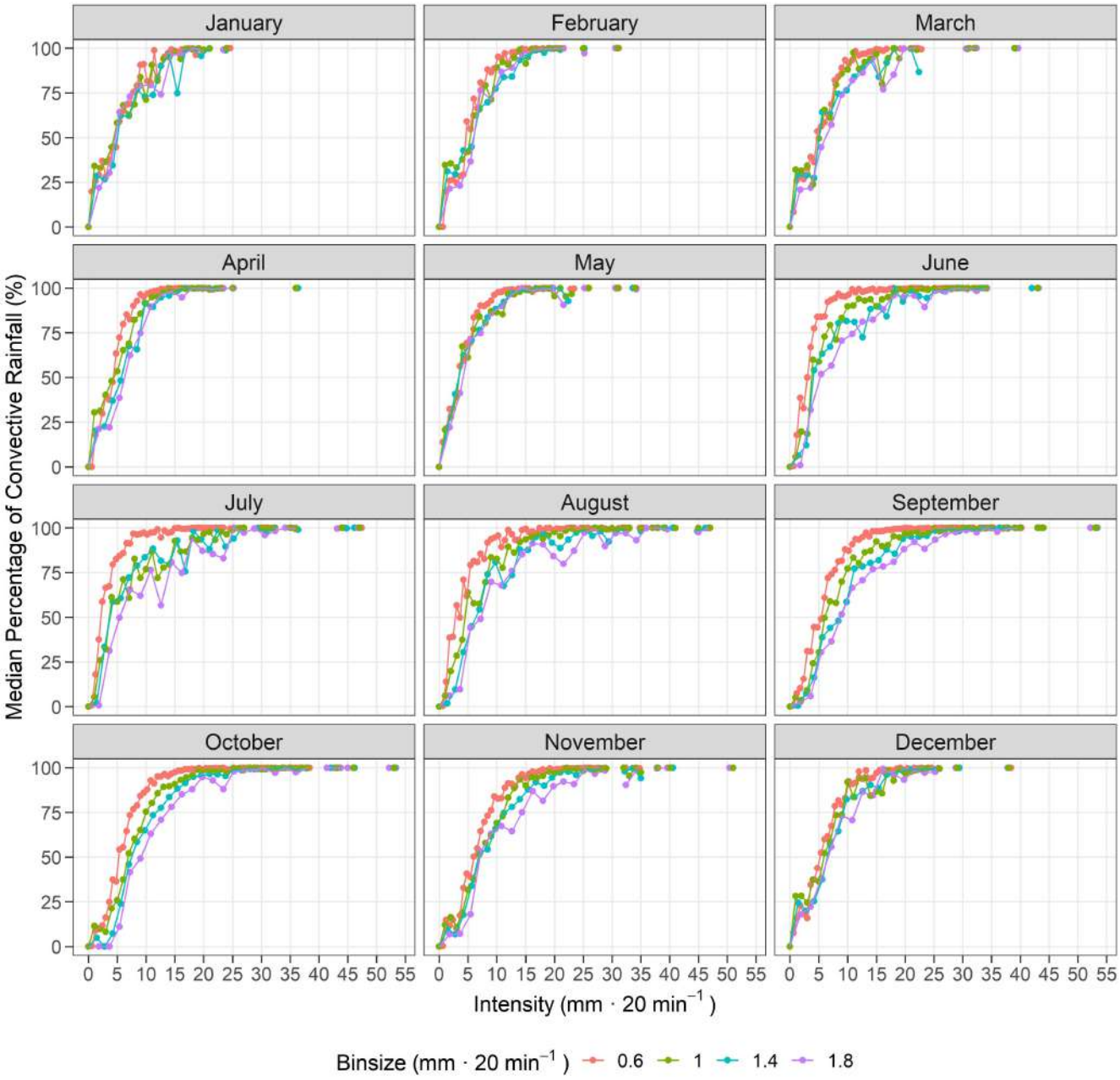

FIGURE 5 Median percentage of convective rainfall with respect to the intensity class, as a function of the month (e.g., the panels) and the ΔI (e.g., the colours). In particular, red, green, blue and purple curve stands for 0.6, 1, 1.4 and, 1.8 mm·20 min^{-1}, respectively [Colour figure can be viewed at wileyonlinelibrary.com]

negative exponential curve. This aspect would determine, in turn, an overestimation of the convective component especially for the lower intensities, since a great number of local peaks result in overfitting of the negative exponential law, as highlighted by Ruiz-Leo *et al.* (2013). Indeed, too much low ΔI lead to a greater variability of $P_T(I)$ even for low-intensity values, thus resulting in an increased probability that no values are present in that classes. This aspect tends to excessively raise the b parameter of the negative exponential curve, and, in turn, to generate a high convective amount at all intensities, misrepresenting the outcome of the algorithm. On the other side of the spectrum, the wider the ΔI, the greater the probability that the $P_T(I)$ is over-discretized. Evidence of this aspect can be noticed considering the 21–25 January interval for all the considered ΔI (i.e., panels a_1, b_1, and c_1). Indeed, considering panel a_1 (e.g., 0.6 mm·20 min^{-1}), there is an almost perfect overlap between $P_T(I)$ and the negative exponential curve, while moving to panel c_1 (e.g., 1.8 mm·20 min^{-1}) the fitting has been avoided, since forcing the curve for less than 4 points would have probably led to unrealistic results. Focusing on panel b_1, instead, it is possible to observe that the differences between $P_T(I)$ and the negative exponential curve are caused by the mathematical framework of the algorithm and result in an overestimation of the convective amount of rainfall in the first class of intensity, as suggested by Ruiz-Leo *et al.* (2013).

For this reason, a consequence of the choice of a wider ΔI is the decreasing capacity of the algorithm to separate the regimes at the lower intensity class.

Ruiz-Leo *et al.* (2013) and Feloni *et al.* (2019) suggested calculating the percentage of convective rainfall as the integral of the area between the total and the stratiform curve. Here a different procedure is suggested, taking into account the differences between various intensity classes or, in other words, giving importance to the atmospheric processes that support the formation of convective rainfall. In particular, considering a generic 5-day distribution, the percentage of convective rainfall can be derived as the ratio between convective and total precipitation for each intensity class considered. Once this process has been repeated for all the 5-day distributions in the period 2002–2020, it is possible to have a sample of convective rainfall percentages for all the intensity classes taken into account.

Figure 5 shows the median value of the percentage of convective rainfall as a function of the intensity class, for fixed the month (e.g., the panels) and the ΔI (e.g., the colours); one can observe that the median value tends to increase moving from low to higher intensities, and this occurs regardless of the month. There is a clear correlation between the highest intensities reached and the months analysed; in particular, from June to November, months have been interested in events characterized by higher intensities (i.e., even more than 30 mm·20 min^{-1}), that are generally classified as convective according to the algorithm here proposed, since the corresponding median percentage of convective rainfall is about 100%. On the contrary, the maximum intensities that characterize the months from December to May are definitely lower, with exception of a few isolated situations.

About the differences among the various ΔI, it is worth noticing that they are significant from June to November while becoming negligible from January to May and in December. The greater variability in the summer/autumn months could be due to the presence of a smaller number of rainfall data recorded, which may reduce the sensitivity of the algorithm in separating the two regimes, especially when high values of ΔI are considered, as stated in section 2.2.3 where the model dependencies have been analysed.

3.3 | Detection of convective events

Once the median values of the percentage of convective rainfall have been identified for each class of intensity, it is possible to derive a median value of the critical intensity threshold I_{cr} for each month and for each ΔI considered. As introduced in section 2.3, the monthly I_{cr} has been derived as the first intensity value which ensures that the median values of the percentage of convective rainfall exceeds a certain limit (hereinafter λ). In particular, two λ have been tested, namely the 50 and 75%. In other words, the monthly I_{cr} can be considered a simple method that allows detecting, at the site scale, those events in which the convective component is predominant at the 50 and 75% on the median behaviour. The use of these two thresholds, instead of 50% only, has been preferred to consider the uncertainty caused by a binary classification of rainfall regimes. Figure 6, which reports the monthly I_{cr} values for (a) $\lambda = 50\%$ and (b) $\lambda = 75\%$ and (1) $\Delta I = 0.6$ mm·20 min^{-1}, (2) $\Delta I = 1$ mm·20 min^{-1}, (3) $\Delta I = 1.4$ mm·20 min^{-1} and, (4) $\Delta I = 1.8$ mm·20 min^{-1}, highlights that the monthly I_{cr} increases as the λ increases, since an event is likely to be classified as convective with more confidence at the higher intensities. Focusing on $\Delta I = 0.6$ mm·20 min^{-1}, a seasonality in the I_{cr} can be observed regardless of the λ considered. As an example, focusing on panel a_1, it is worth to notice that the I_{cr} is lower in July (i.e., about 2.5 mm·20 min^{-1}), while it doubles in January (i.e., about 5 mm·20 min^{-1}). Indeed, it is likely that the convective component is predominant even for lower intensity values during the summer period when it is favoured by higher air temperature

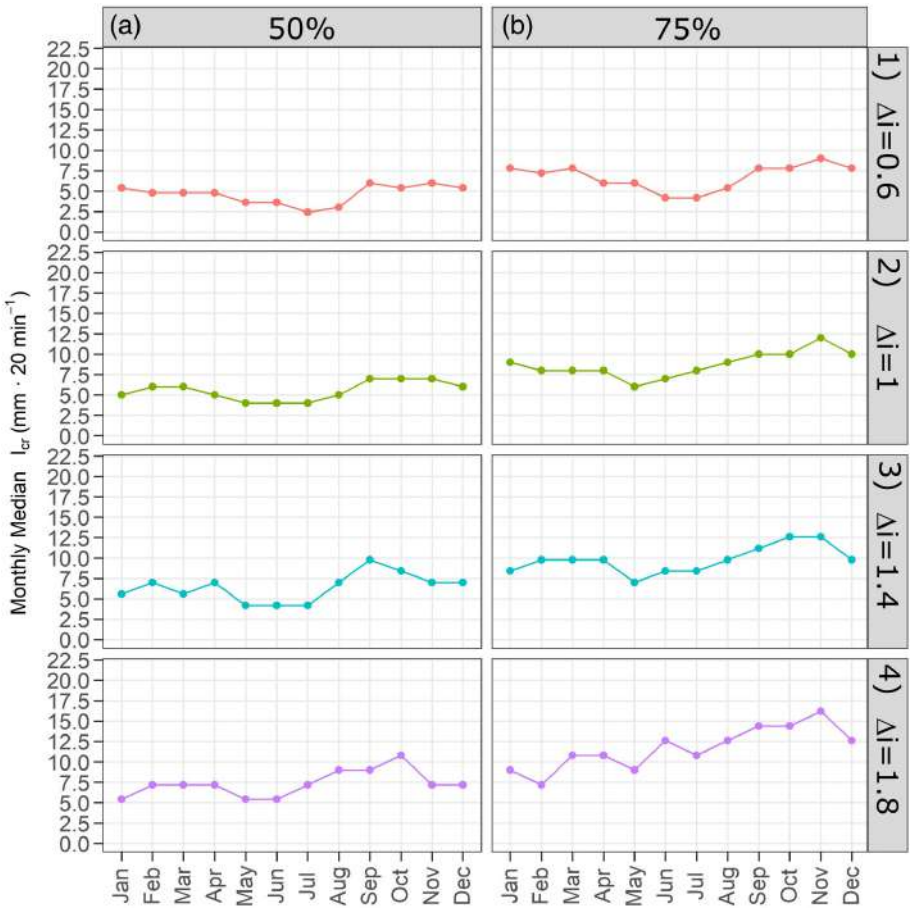

FIGURE 6 Monthly median critical intensity threshold I_{cr} values for (a) $\lambda = 50\%$ and (b) $\lambda = 75\%$ considering (1) $\Delta I = 0.6$ mm·20 min^{-1}, (2) $\Delta I = 1$ mm·20 min^{-1}, (3) $\Delta I = 1.4$ mm·20 min^{-1}, and (4) $\Delta I = 1.8$ mm·20 min^{-1} [Colour figure can be viewed at wileyonlinelibrary.com]

and relative humidity. This behaviour is identifiable also in panel b_1, but with higher intensity values, as previously mentioned. I_{cr} decreases from January to July, where it reaches the minimum for all the λ and then it increases toward the winter months. As opposed to the pattern shown for 0.6 mm·20 min^{-1}, the seasonal behaviour disappears moving to the higher ΔIs and λ. In particular, if on the one hand, it is possible to recognize a similar pattern for $\lambda = 50\%$ and the others ΔIs (i.e., panels a_2, a_3, and a_4), the interseasonal variability of I_{cr} appears excessively high considering $\lambda = 75\%$. As previously introduced, this behaviour is due to a loss of sensitivity of the algorithm in identifying convective rainfall as the ΔI parameter increases, which could lead to a misclassification of convective events (i.e., classifying as convective events that may be mainly stratiform or vice versa).

Considering the results shown in Figures 5 and 6, therefore, the monthly median I_{cr} values for $\Delta I = 0.6$ mm·20 min^{-1} have been chosen for the at-site classification and so used to identify the convective events in the 20-min time series for all the gauges considered. In particular, all the events characterized by rainfall depth greater than the corresponding monthly median I_{cr} values are considered as convective, while the others are supposed to be mainly stratiform. Nevertheless, a further consideration when defining convective events needs to be carried out. Differently from the previous works where the time series are characterized by a 6-hr time resolution, the data here used have a higher temporal frequency (i.e., 20-min), implying that continuous exceedances of I_{cr} may refer to the same convective event. To preserve the condition of independence for the identified events, it has been imposed that the two consecutive convective events must be separated by a minimum duration of 1 hr to be considered independent (Sottile *et al.*, 2021). Once this aggregation procedure is applied, for each convective event is possible to derive (i) the peak of the event (i.e., as the maximum value recorded) and (ii) the total convective precipitation (i.e., the sum of all the values that exceed I_{cr}).

Figure 7 summarizes the results obtained through this detecting procedure. In particular, panel (a) displays an example of the aggregation procedure for the Catania rain gauge. As it is possible to observe, considering the I_{cr} value for $\lambda = 50\%$, $\Delta I = 0.6$ mm·20 min^{-1} and the related month, two different convective events can be identified on the 16th of November 2018. With this in mind, by considering the ensemble of the ground stations that have worked continuously since 2006, panels (b_1) and

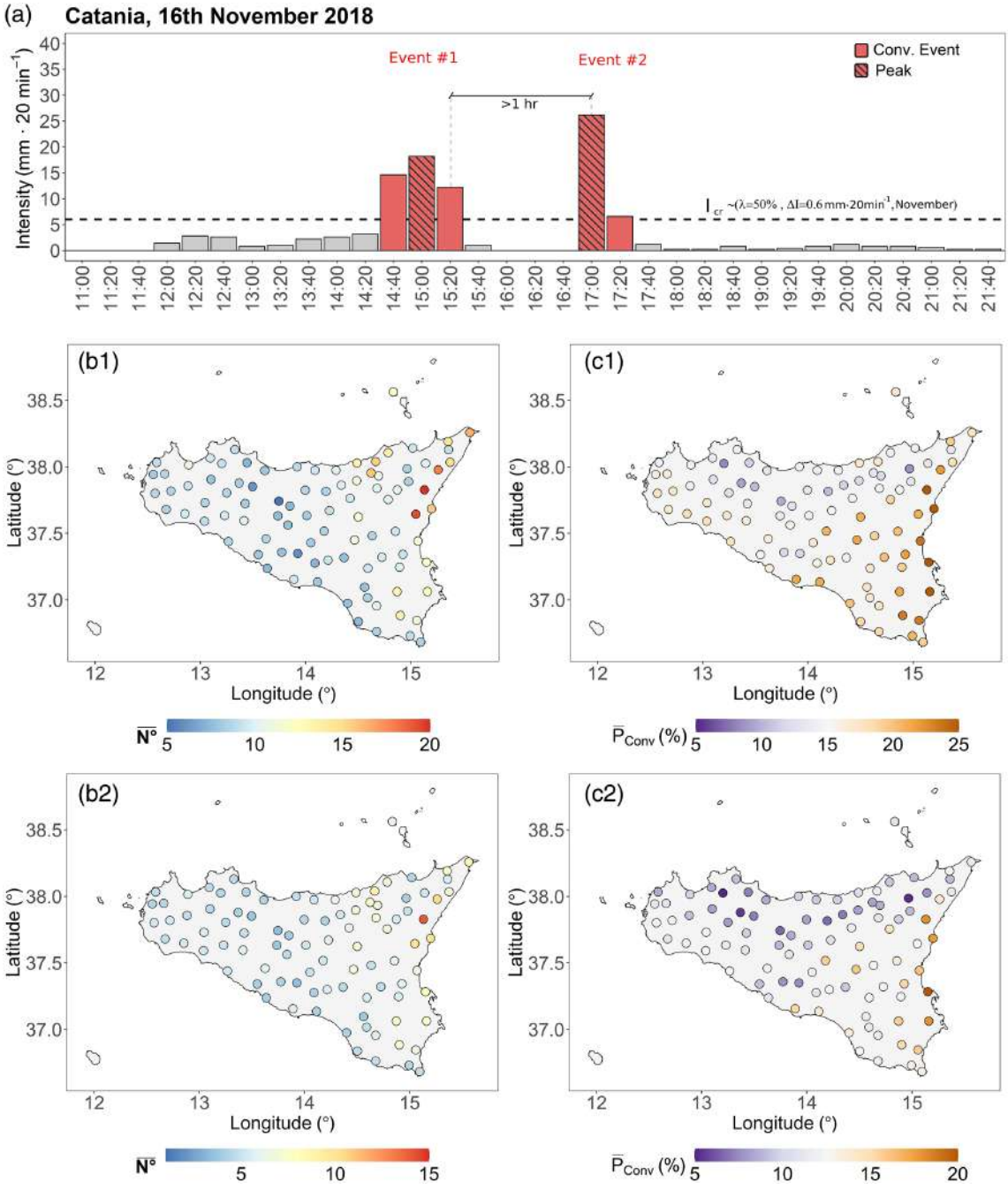

FIGURE 7 Example of the aggregation procedure (a) related to 16th of November 2018 for Catania rain gauge considering the I_{cr} value for $\lambda = 50\%$, $\Delta I = 0.6$ mm·20 min^{-1} and November. The other panels show the spatial distribution of (b) the average annual occurrence of convective events and (c) the average annual percentage of convective rainfall for (1) $\lambda = 50\%$ and (2) $\lambda = 75\%$, obtained by considering the monthly median I_{cr} related to 0.6 mm·20 min^{-1} [Colour figure can be viewed at wileyonlinelibrary.com]

(b_2) show the at-site annual average number of events classified as convective considering $\lambda = 50\%$ and $\lambda = 75\%$, respectively; panels (c_1) and (c_2), instead, show the at-site annual average percentage of convective rainfall for the same λ. Both latter variables have been obtained by averaging the annual values for each station and, for sake of completeness, their spatial distribution in each year considered is reported in Figures S1–S4, Supporting Information.

On the base of the average occurrence of convective events (i.e., panels a_1 and a_2), Sicily could be divided into two zones: the west and central part of the island, generally interested by few convective events in a year (i.e., from five to about 10 on average for $\lambda = 50\%$, but

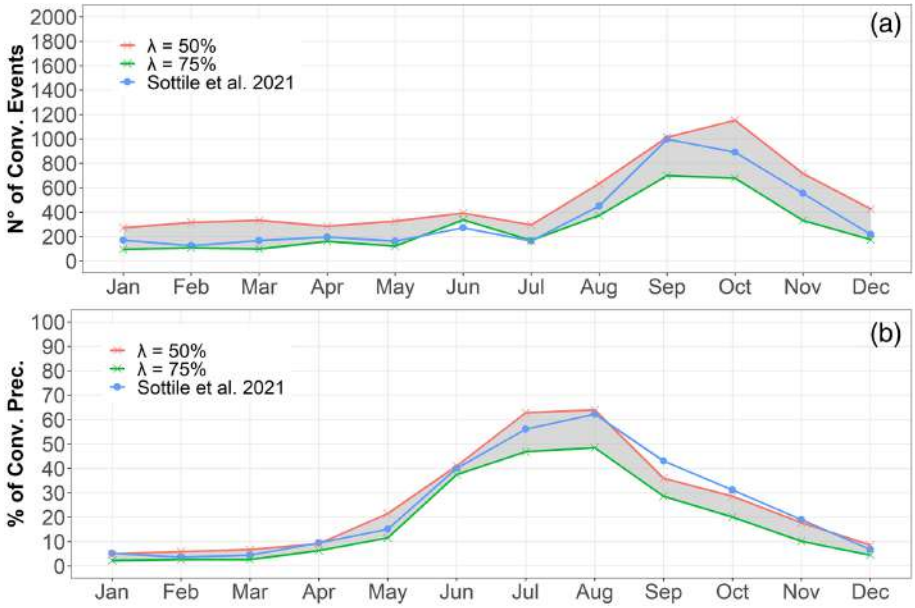

FIGURE 8 Comparison between (a) the monthly absolute number of convective events and (b) the monthly percentage of convective precipitation using $\lambda = 50\%$ and $\lambda = 75\%$ (i.e., the red and green curve, respectively) and the outcomes obtained from Sottile *et al.* (2021) (i.e., the blue curve). The grey shaded area represents the differences between the two λ [Colour figure can be viewed at wileyonlinelibrary.com]

this number decreases considering panel a_2), and the east side, where most of these kinds of events are concentrated. In particular, by looking at the eastern and the northeastern zone it is worth to notice that an important number of stations is characterized by more than 10 convective events per year on average.

Moving to the spatial distribution of the average annual percentage of convective rainfall (panels b_1 and b_2), a similar pattern can be observed. Even in this case, most of the gauges with the highest average annual percentage of convective rainfall for each λ are in the eastern part of the island. This outcome was partially expected due to the presence of the Etna volcano and the Peloritani and Nebrodi mountains in this area; indeed, the warm and humid air coming from the south, especially during the summer, runs into this orographic barrier and cools rapidly as it lifts, thus generating convective heavy rainfall (Caccamo *et al.*, 2017). Nevertheless, this result is alarming since the catchments in the Peloritani mountains have morphological characteristics that make convective events even more dangerous, increasing the risk of flash floods or debris flows (Aronica *et al.*, 2012; Arnone *et al.*, 2016).

3.3.1 | Results comparison with Sottile et al. (2021)

Before performing the trend analysis, the results' consistency has been verified by comparing them with Sottile *et al.* (2021) outcomes. It is worth to specify that Sottile *et al.* (2021) used classification of the rainfall regimes into four classes (i.e., "definitely convective," "possible convective," "slightly convective," and "stratiform") and, for this reason, it has been first necessary to relate these categories to binary classification. In particular, the "definitely convective" and "possible convective" events are here considered as belonging to the convective regime, while the other to the stratiform one. To ensure a coherent comparison, the only rain gauges common to both works (i.e., 40 stations) have been selected over the same operating period (i.e., 2002–2018). Figure 8 provides a comparison between (a) the monthly absolute number of convective events and (b) the monthly percentage of convective precipitation using $\lambda = 50\%$ and $\lambda = 75\%$ depicted by the red and green curves, respectively, and the outcomes obtained from Sottile *et al.* (2021) identified by the blue curve.

As it is possible to observe from both the panels, the seasonal behaviour of the two variables is caught and maintained from the proposed approach. More specifically, for both the classifications, panel (a) shows that the highest values in the occurrence of convective events occur in September/October (i.e., from about 700 to 1,200 convective events per month affect Sicily in the period 2002–2018). Moving to panel (b), instead, the highest percentages of convective rainfall affect the summer season (i.e., from 50 to 60%). The apparent contrast between the position of the peaks in the latter panels is justified by the fact that the greater number of convective events generally recorded in the autumn is balanced by a greater amount of stratiform precipitation; summer months, instead, are generally drier, but the limited number of events that characterize these seasons are probably predominantly convective.

Another aspect that deserves to be considered is that the curves related to Sottile *et al.* (2021) lie between

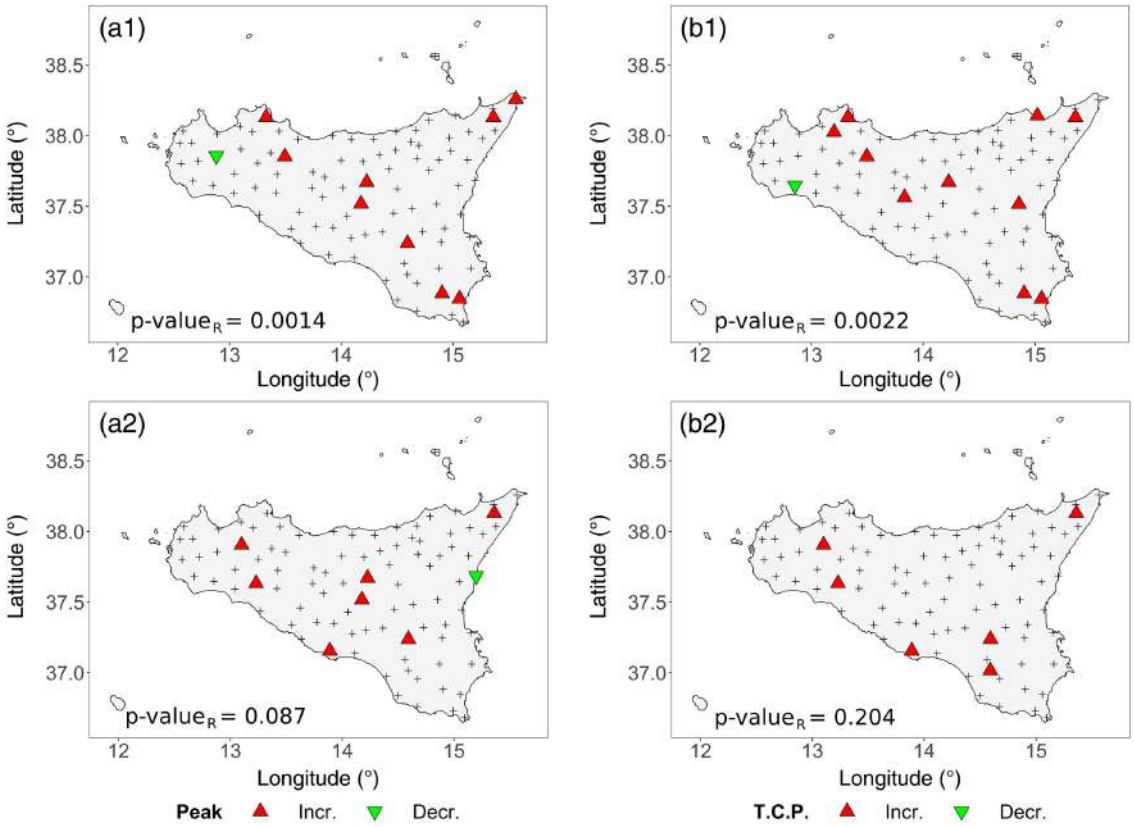

FIGURE 9 Trend analysis results for (a) the peak of convective events and (b) the total convective precipitation for (1) $\lambda = 50\%$ and (2) $\lambda = 75\%$. The cross symbol stands for the gauges where no significant trend has been detected, while the coloured triangles pointing up (pointing down) represents the gauges interested by a significant increasing (decreasing) trend. The *p*-value from the regional Kendall test is shown in the bottom-left corner of each panel [Colour figure can be viewed at wileyonlinelibrary.com]

$\lambda = 50\%$ and $\lambda = 75\%$ for almost every month. In particular only one point is outside the shaded area in panel (a) (i.e., the one related to June), even if the local pattern, that is, the presence of a peak in June, is captured by the proposed method.

3.3.2 | At-site and regional trend analysis

Finally, Figure 9 shows the Mann–Kendall trend analysis results, carried out using a level of significance equal to 0.1, for the peak of convective events (i.e., panels a_1 and a_2) and the total convective precipitation (i.e., panels b_1 and b_2), considering $\lambda = 50\%$ and $\lambda = 75\%$. In all the panels, the cross symbol points out the gauges where no significant trend has been detected, while the coloured triangles pointing up (pointing down) represent the gauges interested by a significant increasing (decreasing) trend.

Observing the findings of the trend analysis, it is possible to notice that about 90% of the gauges are characterized by the absence of any trend for both the variables considered. Nevertheless, when detected, the general behaviour of the significant trend is related to an increase in the considered variable, as evidenced in previous works albeit with different methods and datasets (Arnone *et al.*, 2013; Treppiedi *et al.*, 2021). Moreover, considering panels (a_1) and (b_1), two possible clusters of sites showing increasing trends are maintained for both the variables: the largest one connects the northwest to the southeast corner, while the second one is related to the Peloritani area (i.e., the northeast zone). The regional Kendall test has been applied to check if a general behaviour in the trend direction can be identified through the whole region. It has been obtained that the null hypothesis (i.e., no trend detected) has been rejected for the peak of convective events considering $\lambda = 50\%$ and $\lambda = 75\%$, considering a level of significance equal to 0.05 and 0.1, respectively. Hence, there is evidence for a significant concordance in the trend signs considering the whole region. Indeed, the most of stations shows a positive sign, even if for the at-site Mann–Kendall test it is significant only for only a limited number of them. In the case of the total convective precipitation, instead, it has been found that a positive trend can be identified for $\lambda = 50\%$ (i.e., level of significance equal to 0.05), while it is not

significant for $\lambda = 75\%$. The associated p-values are reported in the bottom-left corner of each panel in Figure 9.

4 | CONCLUSIONS

Separating convective and stratiform rainfall is still today an open challenge, especially because of the difficulty in defining a clear distinction between the two rainfall components. At the same time, the study of convective rainfall is essential to better understand the dynamics that generate them and to plan proactive measures that could reduce the risk of important consequences (e.g., human life losses and economic damages). The shadow of a changing climate makes these aspects even more alarming, due to the possibility of an increase in the occurrence of such severe events.

In this work, the algorithm proposed by Tremblay (2005) has been modified and applied to separate the convective and the stratiform regime at the monthly scale for Sicily (Italy). Starting from a high-resolution regional rainfall dataset, provided by the SIAS for the period 2002–2020, the 20-min precipitation time series have been grouped in a certain number of intensity classes, to derive the 5-day total precipitation distribution. This curve, describing how the total precipitation depth tends to decrease with the intensity, allows to model the stratiform component as a negative exponential law and, consequentially, to obtain for the difference the convective one for each class of intensity. The application of the model involved some modifications together with a careful analysis of its dependencies, such as the sample numerosity, the average time interval of reference and, the intensity bin size, namely ΔI. In particular, while the previous studies based on this algorithm used an empirical method for choosing the ΔI, in this work a sensitivity analysis of this parameter has been carried out with the aim not to find its "optimal" value, but to analyse its influence on the results.

It has been found that the algorithm provides results that are consistent with previous studies, namely that the median percentage of convective rainfall tends to increase as the intensity increases, regardless of the month considered. Nevertheless, it has been found that for some fixed percentages, the related intensity is lower in the summer months with respect to the other seasons, especially for the lowest ΔI considered. From a physical point of view, this aspect could be motivated by the fact that, during these months, the convective regime results predominant even for lower intensities due to the higher air temperature and relative humidity that characterized the Mediterranean climate.

The monthly critical intensity thresholds I_{cr} have been defined to move from the regional to the at-site spatial scale. For each month, the threshold has been derived as the first intensity value that overcomes a median percentage of convective rainfall equal to 50 and 75%. Indeed, the higher the latter limit, the "more convective" the event that is identified. Indeed, representing the value of intensity from which the convective regime starts prevailing on the stratiform one, this threshold allows for detecting the convective events from the 20-min time series for each gauge under study. In particular, once the convective events are clustered, some related variables have been extracted from the series, namely the peak (i.e., the maximum intensity value) and the total convective precipitation, and calculated for each point of measurement, namely the annual occurrence (i.e., the number of exceedances in a year) and the annual percentage of convective rainfall. By averaging the latter two variables over the considered period, it has been noticed that the east side of the island is the most affected by convective events, probably due to the orography of that area. Moreover, the morphological characteristics of this part of the island make this aspect more alarming about the attitude toward generating flash floods and debris flows. The results obtained through this framework are also consistent with those provided by Sottile *et al.* (2021). Indeed, both the classifications reveal a seasonality in the occurrence of convective events and the percentage of convective rainfall. In particular, summer months are characterized by higher values of convective rainfall, while the most convective events occur in September and October. Finally, by applying an at-site trend analysis on the peak and the total convective precipitation values, it has been found that most of the gauges do not reveal significant trends, despite the greatest part of the significant ones shows an increasing sign, that is, an increase in the convective rainfall in those sites.

DATA AVAILABILITY STATEMENT

Dataset related to this article has been provided by the regional agency SIAS (Servizio Informativo Agrometeorologico Siciliano) through a formal request (http://www.sias.regione.sicilia.it/).

ORCID

Dario Treppiedi https://orcid.org/0000-0002-1359-1650

REFERENCES

Ali, H., Fowler, H.J., Lenderink, G., Lewis, E. and Pritchard, D. (2021) Consistent large-scale response of hourly extreme precipitation to temperature variation over land. *Geophysical Research Letters*, 48, e2020GL090317. https://doi.org/10.1029/2020GL090317.

Arnone, E., Dialynas, Y.G., Noto, L.V. and Bras, R.L. (2016) Accounting for soil parameter uncertainty in a physically based and distributed approach for rainfall-triggered landslides. *Hydrological Processes*, 30(6), 927–944. https://doi.org/10.1002/hyp.10609.

Arnone, E., Pumo, D., Francipane, A., La Loggia, G. and Noto, L.V. (2018) The role of urban growth, climate change, and their interplay in altering runoff extremes. *Hydrological Processes*, 32, 1755–1770. https://doi.org/10.1002/hyp.13141.

Arnone, E., Pumo, D., Viola, F., Noto, L. and la Loggia, G. (2013) Rainfall statistics in Sicily. *Hydrology and Earth System Sciences*, 10, 2449–2458. https://doi.org/10.5194/hess-17-2449-2013.

Aronica, G., Cannarozzo, M. and Noto, L. (2002) Investigating the changes in extreme rainfall series recorded in an urbanised area. *Water Science and Technology*, 45, 49–54. https://doi.org/10.2166/wst.2002.0026.

Aronica, G.T., Brigandí, G. and Morey, N. (2012) Flash floods and debris flow in the city area of Messina, north-east part of Sicily, Italy in October 2009: the case of the Giampilieri catchment. *Natural Hazards and Earth System Sciences*, 12, 1295–1309. https://doi.org/10.5194/nhess-12-1295-2012.

Bartolini, G., Grifoni, D., Torrigiani, T., Vallorani, R., Meneguzzo, F. and Gozzini, B. (2014) Precipitation changes from two long-term hourly datasets in Tuscany, Italy. *International Journal of Climatology*, 34, 3977–3985. https://doi.org/10.1002/joc.3956.

Berg, P., Moseley, C. and Haerter, J.O. (2013) Strong increase in convective precipitation in response to higher temperatures. *Nature Geoscience*, 6, 181–185. https://doi.org/10.1038/ngeo1731.

Borga, M., Boscolo, P., Zanon, F., Sangati, M., Borga, M., Boscolo, P., Zanon, F. and Sangati, M. (2007) Hydrometeorological analysis of the August 29, 2003 flash flood in the eastern Italian Alps. *Journal of Hydrometeorology*, 8, 1049–1067. https://doi.org/10.1175/jhm593.1.

Caccamo, M.T., Castorina, G., Colombo, F., Insinga, V., Maiorana, E. and Magazù, S. (2017) Weather forecast performances for complex orographic areas: impact of different grid resolutions and of geographic data on heavy rainfall event simulations in Sicily. *Atmospheric Research*, 198, 22–33. https://doi.org/10.1016/j.atmosres.2017.07.028.

Cannarozzo, M., Noto, L.V. and Viola, F. (2006) Spatial distribution of rainfall trends in Sicily (1921–2000). *Physics and Chemistry of the Earth, Parts A/B/C*, 31, 1201–1211. https://doi.org/10.1016/j.pce.2006.03.022.

Cipolla, G., Francipane, A. and Noto, L.V. (2020) Classification of extreme rainfall for a Mediterranean region by means of atmospheric circulation patterns and reanalysis data. *Water Resources Management*, 34, 3219–3235. https://doi.org/10.1007/s11269-020-02609-1.

Di Piazza, A., Conti, F.L., Noto, L.V., Viola, F. and La Loggia, G. (2011) Comparative analysis of different techniques for spatial interpolation of rainfall data to create a serially complete monthly time series of precipitation for Sicily, Italy. *International Journal of Applied Earth Observation and Geoinformation*, 13, 396–408. https://doi.org/10.1016/j.jag.2011.01.005.

Donat, M.G., Lowry, A.L., Alexander, L.V., O'Gorman, P.A. and Maher, N. (2016) More extreme precipitation in the world's dry and wet regions. *Nature Climate Change*, 6, 508–513. https://doi.org/10.1038/nclimate2941.

Douglas, E.M., Vogel, R.M. and Kroll, C.N. (2000) Trends in floods and low flows in the United States: impact of spatial correlation. *Journal of Hydrology*, 240, 90–105. https://doi.org/10.1016/S0022-1694(00)00336-X.

Feloni, E., Baltas, E., Nastos, P. and Matsangouras, I. (2019) Implementation and evaluation of a convective/stratiform precipitation scheme in Attica region, Greece. *Atmospheric Research*, 220, 109–119.

Forestieri, A., Arnone, E., Blenkinsop, S., Candela, A., Fowler, H. and Noto, L.V. (2018) The impact of climate change on extreme precipitation in Sicily, Italy. *Hydrological Processes*, 32, 332–348. https://doi.org/10.1002/hyp.11421.

Forestieri, A., Caracciolo, D., Arnone, E. and Noto, L.V. (2016) Derivation of rainfall thresholds for flash flood warning in a Sicilian Basin using a hydrological model. *Procedia Engineering*, 154, 818–825.

Fowler, H.J., Lenderink, G., Prein, A.F., Westra, S., Allan, R.P., Ban, N., Barbero, R., Berg, P., Blenkinsop, S., Do, H.X., Guerreiro, S., Haerter, J.O., Kendon, E.J., Lewis, E., Schaer, C., Sharma, A., Villarini, G., Wasko, C. and Zhang, X. (2021) Anthropogenic intensification of short-duration rainfall extremes. *Nature Reviews Earth & Environment*, 2, 107–122. https://doi.org/10.1038/s43017-020-00128-6.

Francipane, A., Pumo, D., Sinagra, M., La Loggia, G. and Noto, L.V. (2021) A paradigm of extreme rainfall pluvial floods in complex urban areas: the flood event of July 15, 2020 in Palermo (Italy). *Natural Hazards and Earth System Sciences*, 2021, 1–32. https://doi.org/10.5194/nhess-2021-61.

Hardwick Jones, R., Westra, S. and Sharma, A. (2010) Observed relationships between extreme sub-daily precipitation, surface temperature, and relative humidity. *Geophysical Research Letters*, 37, L22805. https://doi.org/10.1029/2010GL045081.

Helsel, D.R. and Frans, L.M. (2006) Regional Kendall test for trend. *Environmental Science & Technology*, 40, 4066–4073. https://doi.org/10.1021/es051650b.

Houze, R.A. (1993) *Cloud Dynamics*. International Geophysics Series, Vol. 53, pp. 11–29. https://www.elsevier.com/books/cloud-dynamics/houze-jr/978-0-12-356880-9

Houze, R.A. (1997) Stratiform precipitation in regions of convection: a meteorological paradox? *Bulletin of the American Meteorological Society*, 78, 2179–2196. https://doi.org/10.1175/1520-0477(1997)078<2179:SPIROC>2.0.CO;2.

IPCC. (2019) In: Shukla, P.R., Skea, J., Buendia, E.C., Masson-Delmotte, V., Pörtner, H.-O., Roberts, D.C., Zhai, P., Slade, R., Connors, S., van Diemen, R., Ferrat, M., Haughey, E., Luz, S., Neogi, S., Pathak, M., Petzold, J., Pereira, J.P., Vyas, P., Huntley, E., Kissick, K., Belkacemi, M. and Malley, J. (Eds.) *Climate Change and Land: An IPCC Special Report on Climate Change, Desertification, Land Degradation, Sustainable Land Management, Food Security, and Greenhouse Gas Fluxes in Terrestrial Ecosystems*, (in press). https://www.ipcc.ch/srccl/cite-report/

Kendall, M.G. (1948) *Rank correlation methods*. Oxford, England: Griffin.

Kolios, S. and Feidas, H. (2010) A warm season climatology of mesoscale convective systems in the Mediterranean basin using

satellite data. *Theoretical and Applied Climatology*, 102, 29–42. https://doi.org/10.1007/s00704-009-0241-7.

Kundzewicz, Z.W. (2008) Climate change impacts on the hydrological cycle. *Ecohydrology & Hydrobiology*, 8, 195–203. https://doi.org/10.2478/v10104-009-0015-y.

Kyselý, J., Beguería, S., Beranová, R., Gaál, L. and López-Moreno, J. I. (2012) Different patterns of climate change scenarios for short-term and multi-day precipitation extremes in the Mediterranean. *Global and Planetary Change*, 98–99, 63–72. https://doi.org/10.1016/j.gloplacha.2012.06.010.

Kyselý, J., Rulfová, Z., Farda, A. and Hanel, M. (2016) Convective and stratiform precipitation characteristics in an ensemble of regional climate model simulations. *Climate Dynamics*, 46, 227–243. https://doi.org/10.1007/s00382-015-2580-7.

Lenderink, G. and van Meijgaard, E. (2008) Increase in hourly precipitation extremes beyond expectations from temperature changes. *Nature Geoscience*, 1, 511–514. https://doi.org/10.1038/ngeo262.

Lionello, P. and Scarascia, L. (2018) The relation between climate change in the Mediterranean region and global warming. *Regional Environmental Change*, 18, 1481–1493. https://doi.org/10.1007/s10113-018-1290-1.

Llasat, M.-C. (2001) An objective classification of rainfall events on the basis of their convective features: application to rainfall intensity in the northeast of Spain. *International Journal of Climatology*, 21, 1385–1400. https://doi.org/10.1002/joc.692.

Llasat, M.C., del Moral, A., Cortès, M. and Rigo, T. (2021) Convective precipitation trends in the Spanish Mediterranean region. *Atmospheric Research*, 257, 105581. https://doi.org/10.1016/j.atmosres.2021.105581.

Mann, H.B. (1945) Nonparametric tests against trend. *Econometrica*, 13, 245–259.

Michaelides, S., Karacostas, T., Sánchez, J.L., Retalis, A., Pytharoulis, I., Homar, V., Romero, R., Zanis, P., Giannakopoulos, C., Bühl, J., Ansmann, A., Merino, A., Melcón, P., Lagouvardos, K., Kotroni, V., Bruggeman, A., López-Moreno, J.I., Berthet, C., Katragkou, E., Tymvios, F., Hadjimitsis, D.G., Mamouri, R.-E. and Nisantzi, A. (2018) Reviews and perspectives of high impact atmospheric processes in the Mediterranean. *Atmospheric Research*, 208, 4–44. https://doi.org/10.1016/j.atmosres.2017.11.022.

Morel, C. and Senesi, S. (2002) A climatology of mesoscale convective systems over Europe using satellite infrared imagery. II: characteristics of European mesoscale convective systems. *Quarterly Journal of the Royal Meteorological Society*, 128, 1973–1995. https://doi.org/10.1256/003590002320603494.

Muñoz-Díaz, D. and Rodrigo, F.S. (2006) Seasonal rainfall variations in Spain (1912–2000) and their links to atmospheric circulation. *Atmospheric Research*, 81, 94–110. https://doi.org/10.1016/j.atmosres.2005.11.005.

Nastos, P.T., Matsangouras, I.T. and Chronis, T.G. (2014) Spatio-temporal analysis of lightning activity over Greece—preliminary results derived from the recent state precision lightning network. *Atmospheric Research*, 144, 207–217. https://doi.org/10.1016/j.atmosres.2013.10.021.

NOAA. (2012) Severe weather 101-thunderstorm types. Available at: https://www.nssl.noaa.gov/education/svrwx101/thunderstorms/types/.

Pumo, D., Arnone, E., Francipane, A., Caracciolo, D. and Noto, L. V. (2017) Potential implications of climate change and urbanization on watershed hydrology. *Journal of Hydrology*, 554, 80–99. https://doi.org/10.1016/j.jhydrol.2017.09.002.

Reudenbach, C., Heinemann, G., Heuel, E., Bendix, J. and Winiger, M. (2001) Investigation of summertime convective rainfall in Western Europe based on a synergy of remote sensing data and numerical models. *Meteorology and Atmospheric Physics*, 76, 23–41. https://doi.org/10.1007/s007030170037.

Rigo, T. and Llasat, M.C. (2004) A methodology for the classification of convective structures using meteorological radar: application to heavy rainfall events on the Mediterranean coast of the Iberian Peninsula. *Natural Hazards and Earth System Sciences*, 4, 59–68. https://doi.org/10.5194/nhess-4-59-2004.

Rigo, T. and Llasat, M.-C. (2007) Analysis of mesoscale convective systems in Catalonia using meteorological radar for the period 1996–2000. *Atmospheric Research*, 83, 458–472. https://doi.org/10.1016/j.atmosres.2005.10.016.

Ruiz-Leo, A.M., Hernandez, E., Queralt, S. and Maqueda, G. (2013) Convective and stratiform precipitation trends in the Spanish Mediterranean coast. *Atmospheric Research*, 119, 46–55.

Rulfová, Z. and Kyselý, J. (2013) Disaggregating convective and stratiform precipitation from station weather data. *Atmospheric Research*, 134, 100–115. https://doi.org/10.1016/j.atmosres.2013.07.015.

Rulfová, Z. and Kyselý, J. (2014) Trends of convective and stratiform precipitation in the Czech Republic, 1982–2010. *Advances in Meteorology*, 2014, 647938. https://doi.org/10.1155/2014/647938.

Sandford, C., Illingworth, A. and Thompson, R. (2017) The potential use of the linear depolarization ratio to distinguish between convective and stratiform rainfall to improve radar rain-rate estimates. *Journal of Applied Meteorology and Climatology*, 56, 2927–2940.

Scoccimarro, E., Gualdi, S., Bellucci, A., Zampieri, M. and Navarra, A. (2013) Heavy precipitation events in a warmer climate: results from CMIP5 models. *Journal of Climate*, 26, 7902–7911.

Sottile, G., Francipane, A., Adelfio, G. and Noto, L.V. (2021) A PCA-based clustering algorithm for the identification of stratiform and convective precipitation at the event scale: an application to the sub-hourly precipitation of Sicily, Italy. In: *Stochastic Environmental Research and Risk Assessment*. https://doi.org/10.1007/s00477-021-02028-7.

Steiner, M., Houze, R.A. and Yuter, S.E. (1995) Climatological characterization of three-dimensional storm structure from operational radar and rain gauge data. *Journal of Applied Meteorology*, 34, 1978–2007.

Tremblay, A. (2005) The stratiform and convective components of surface precipitation. *Journal of the Atmospheric Sciences*, 62, 1513–1528.

Trenberth, K.E. (2011) Changes in precipitation with climate change. *Climate Research*, 47, 123–138. https://doi.org/10.3354/cr00953.

Treppiedi, D., Cipolla, G., Francipane, A. and Noto, L.V. (2021) Detecting precipitation trend using a multiscale approach based on quantile regression over a Mediterranean area. *International Journal of Climatology*, 41, 5938–5955. https://doi.org/10.1002/joc.7161.

Westra, S., Fowler, H.J., Evans, J.P., Alexander, L.V., Berg, P., Johnson, F., Kendon, E.J., Lenderink, G. and Roberts, N.M. (2014) Future changes to the intensity and frequency of short-duration extreme rainfall. *Reviews of Geophysics*, 52, 522–555. https://doi.org/10.1002/2014RG000464.

SUPPORTING INFORMATION

Additional supporting information can be found online in the Supporting Information section at the end of this article.

How to cite this article: Treppiedi, D., Cipolla, G., & Noto, L. V. (2023). Convective precipitation over a Mediterranean area: From identification to trend analysis starting from high-resolution rain gauges data. *International Journal of Climatology*, *43*(1), 293–313. https://doi.org/10.1002/joc.7758